Thermal and structural response of *in situ* prepared biobased poly(ethylene 2,5-furan dicarboxylate) nanocomposites

Nadia Lotti[1*], Andrea Munari[1], Matteo Gigli[2], Massimo Gazzano[3],

Vasilios Tsanaktsis[4], Dimitrios N. Bikiaris[4*], George Z. Papageorgiou[5]

[1]Civil, Chemical, Environmental and Materials Engineering Department, University of Bologna, Via Terracini 28, 40131 Bologna, Italy.

[2]Department of Chemical Science and Technology, University of Roma "Tor Vergata", Via della Ricerca Scientifica 1, 00133 Roma, Italy (present address, work done at address 1).

[3]Organic Synthesis and Photoreactivity Institute, CNR, Via Selmi 2, 40126 Bologna, Italy

[4]Laboratory of Polymer Chemistry and Technology, Department of Chemistry, Aristotle University of Thessaloniki, 54124 Thessaloniki, Macedonia, Greece.

[5]Chemistry Department, University of Ioannina, P.O. Box 1186, 45110 Ioannina, Greece.

* Corresponding authors.   Nadia Lotti, E-mail: nadia.lotti@unibo.it

Dimitrios Bikiaris, E-mail: dbic@chem.auth.gr

Abstract

Poly(ethylene 2,5-furan dicarboxylate) (PEF) is considered the biobased counterpart of the fossil based poly(ethylene terephthalate) for food packaging. In this research, PEF nanocomposites containing 2.5 wt% neat multi walled carbon nanotubes (MWCNTs), or functionalized MWCNTs or graphene oxide (GO), were in situ prepared by applying the melt polycondensation method. The nanocomposites showed faster crystallization rates compared to the pristine material as proved by both differential scanning calorimetry (DSC) and polarized light microscopy (PLM). The latter evidenced an increased nucleation density in nanocomposites, due to the nucleating efficiency of the fillers, resulting in smaller spherulite size. However, a slightly reduced thermal stability was revealed for the nanocomposites by thermogravimetric analysis (TGA), especially in the case of GO-containing samples. The solid structure of the materials was studied by performing real time X-ray diffraction (XRD) measurements. In neat PEF, β-crystals were observed in the solvent treated sample, while α-crystals were formed on cooling from the melt or cold-crystallization. On the contrary, in the XRD patterns of the nanocomposites only peaks associated with the α-crystal phase were found. Last, but not least, the effect of recrystallization on the thermal behavior was evaluated by means of modulated temperature DSC (MDSC).

Keywords: Poly(ethylene 2,5 furan dicarboxylate); renewable polymers; PEF crystal structure; nanocomposites; crystallisation.

1. Introduction

Chemicals from vegetable feedstocks have been proposed as monomers for polymer production. Sugars available within the biorefinery can be converted to a family of products, including dehydrosugars, furans, and levulinic acid by dehydration. 2,5-furandicarboxylic acid (2,5-FDCA) is an important member of the furan family that can be formed by an oxidative dehydration of glucose [1]. FDCA can be also produced by oxidation of 5-hydroxymethylfurfural sources [2]. It has a large potential as a replacement for terephthalic acid, a widely used component in various polyesters, such as poly(ethylene terephthalate) (PET), poly(propylene terephthalate) (PPT) and poly(butylene terephthalate) (PBT). PEF is the most studied and most important polyester from 2,5-FDCA. The utility of this biobased polyester as a PET analog offers an important opportunity to address a high volume, high value chemical market.

Roughly, 56 million tons of PET are produced each year [3]. The market value of PET plastic varies, depending on the application, in the range of $1.00 – 3.00/lb. Assuming a mean value of 2.00/lb, it leads to an estimation of 247 billions $/yr for PET market.

Furan based polyesters like PEF have been reported for years [4-6]. However, in the most of these cases, colored low molecular weight polymers were prepared, as result of the FDCA decomposition. Nowadays, there is a growing interest in polyesters bearing furan moieties like PEF and poly(butylene 2,5-furan dicarboxylate) (PBF) from both industry and academics [7-10]. Consequently, a quite high number of papers describe synthesis and characterization of furan polyesters [10-23], even though to date only a few of them report their properties. PEF is undoubtedly the best characterized furan-based polyester, in light of a food packaging application. The results obtained in these studies indicate that it exhibits significantly improved barrier properties compared to PET, justifying its attractiveness. More in detail, amorphous PEF exhibits an 11X reduction in oxygen permeability, a 19X reduction in carbon dioxide permeability, and a 2.1X reduction in water permeability as compared to amorphous PET [24-26].

Moreover, PEF shows beneficial thermal transition temperatures such as a higher T_g and a lower melting temperature, with respect to to PET. Crystallization and melting of PEF have been studied in recent works [27-30] as well as its crystal structure by Kazaryan and Medvedeva, [31] while in recent studies details of crystallization were investigated by means of WAXD and DSC [32, 33]. Recently, enzymatic hydrolysis of PEF was also evaluated [34].

It is well known that high-order structures of polymers, such as chain orientation and crystallites play an important role in enhancing the properties of the film, such as gas barrier and mechanical properties as well as wear resistance [35, 36]. Unfortunately, the slow crystallization rate and moderate crystallinity of PET compared to PBT and PPT restrict its applications, in particular by injection molding [37, 38]. Nano-fillers can be added to enhance mechanical and gas barrier properties, and to improve thermal and dimensional stability of polymers, as proved by PET/clay nanocomposites previously reported [39]. Furthermore, crystallization of PET can be significantly affected by the incorporation of nano-fillers [40-42].

Polymer nanocomposites based on carbon black, carbon nanotubes (CNTs), and layered silicates have been prepared to improve the mechanical, thermal, electrical, and gas barrier properties of neat polymers [43-46]. Traditional composites contain a significant quantity (60 vol%) of filler bound in a polymer matrix. In nanocomposites

dramatic changes in properties are possible at very low filler loadings (< 2 vol%). This depends on the inherent properties of the nanofiller, but also on the dispersion, interface chemistry and nanoscale morphology, which takes advantage of the enormous surface area per unit volume of nanofillers [47]. Nowadays, in nanocomposites research, a lot of emphasis has been given to the study of carbon based nanofillers, mostly CNTs and to a limited extent to graphite. Excellent reviews are available dealing with graphene, chemical methods for the production of graphene and processing of nanographene platelets and the corresponding nanocomposites [48-50]. Long-range π-conjugation in graphene yields extraordinary thermal, mechanical, and electrical properties, which have long been the interest of many theoretical studies and more recently became an exciting area for experimentalists [51, 52]. Graphene oxide is a layered material produced by the oxidation of graphene and thus graphene oxide sheets are oxygenated to a large extent, bearing hydroxyl and epoxide functional groups on their basal planes. Carbonyl and carboxyl groups also appear at the sheet edges and consequently graphene oxide sheets are strongly hydrophilic [53-56].

To the best of our knowledge, no published works reported PEF-nanocomposites, prepared in situ by melt-polycondensation method and containing MWCNTs, with or without functionalization, as well as GO. In this framework, we decided to prepare and characterize these new PEF nanocomposites, in order to investigate the effects of the different nanofillers on the material final properties. More specifically, the nanocomposites were investigated with respect to their crystallization and melting behavior and thermal stability by using WAXD, DSC, MDSC, PLM and TGA.

2. Experimental

2.1. Materials

2,5-furan dicarboxylic acid (purum 97 %), ethylene glycol anhydrous 99.8% (EG) and tetrabutyltitanate (TBT) catalyst of analytical grade were purchased from Aldrich Co. Neat multi-walled carbon nanotubes (MWCNTs) were synthesized by chemical vapor deposition (CVD) process and were supplied by Timesnano Chengdu Organic Chemicals Co. (China). Their diameter was 10–20 nm and their length was about 10 μm. Carboxyl groups functionalized MWCNTs (MWCNTs-COOH) were prepared after oxidation of neat MWCNTs in concentrated nitric and sulfuric acid. MWCNTs (4 g) were suspended in 150 mL of a mixture of concentrated nitric acid and sulfuric acid

(1:3 in volume ratio) and refluxed for 20 min. After washing with deionized water until the supernatant attained a pH around 6, the samples were dried under nitrogen flux at 60 °C [57]. Amino functionalized multi-walled carbon nanotubes (MWCNTs-NH$_2$) were kindly supplied by GLONATECH S.A (Athens Greece, ONEX-MW 1004C2). The nanotubes have 5% -NH$_2$ content, average diameter of 15-35 nm, length > 5 μm and bulk density 0.2 g/cm^3. The GO was produced through a modified Staudenmaier's method [58]. In a typical synthesis, 10 g of powdered graphite were added to a mixture of concentrated sulphuric acid and nitric acid while cooling in an ice-water bath. Potassium chlorate powder was added to the mixture in small portions while stirring and cooling. The reactions were quenched after 18 h by pouring the mixture into distilled water and the oxidation product washed until a pH 6. The sample was then dried at room temperature.

2.2. Synthesis of 2,5-dimethylfuran-dicarboxylate (DMFD)

15.6 g of 2,5-furandicarboxylic acid, 200 mL of anhydrous methanol and 2 mL of concentrated sulfuric acid were transferred into a round bottom flask (500 mL) and the mixture was refluxed for 5 hours. The excess of the methanol was distilled and the solution was filtered through a disposable Teflon membrane filter. During filtration, dimethylester was precipitated as white powder and, after cooling, 100 mL of distilled water was added. The dispersion was partially neutralized by adding Na$_2$CO$_3$ 5 % w/v during stirring, while pH was measured continuously. The white powder was filtered and the solid was washed several times with distilled water and dried. The isolated white dimethylester was recrystallized with a mixture of 50/50 v/v methanol/water. After cooling, 2,5-dimethylfuran-dicarboxylate (DMFD) was precipitated in the form of white needles. The reaction yield was calculated at 83 %.

2.3. PEF and nanocomposites synthesis

PEF was synthesized through the two-stage melt polycondensation (esterification and polycondensation) in a glass batch reactor [27]. DMFD and ethylene glycol in a molar ratio of diester/diol=1/2.2 were charged into the reaction tube of the polyesterification apparatus with 400 ppm of TBT. The reaction mixture was heated at 150 °C under argon flow for 2h, at 160 °C for additional 2h and finally at 170 °C for 1h. This first step (transesterification) is considered complete after the collection of almost all the

theoretical amount of CH$_3$OH, which was removed from the reaction mixture by distillation and collected in a graduate cylinder. In the second step of polycondensation, vacuum (5.0 Pa) was applied slowly over a time of about 30 min to remove the excess of diol, to avoid excessive foaming and to minimize oligomer sublimation, which is a potential problem during the melt polycondensation. The temperature was gradually increased (1h) to 220 °C, while stirring speed was also increased to 720 rpm. The reaction continued at this temperature for 2h. Successively, the temperature was increased to 230 °C for 2h and to 240 °C for additional 1h.

PEF-based nanocomposites containing 2.5 wt% of MWCNTs, MWCNTs-COOH, MWCNTs-NH$_2$ and GO were in situ prepared using also the two stage melt polycondensation method. Nanofillers were added to the ethylene glycol and the dispersion was subjected to sonication for 15 min to obtain a uniform dispersion. Afterwards, the dispersion was added to the reaction tube together with DMFD and TBT catalyst. The reaction continued, as above described for the synthesis of neat PEF. After the polycondensation reaction was completed, neat PEF and its nanocomposites were easily removed, milled and washed with methanol.

2.4. Intrinsic viscosity measurements

Intrinsic viscosity [η] measurements were performed using an Ubbelohde viscometer at 30 °C in a mixture of phenol/1,1,2,2-tetrachloroethane (60/40, w/w). The sample was kept in the above mentioned mixture at 90°C until a complete dissolution was achieved. The solution was then cooled to room temperature and filtered through a Teflon disposable membrane filter.

2.5. Nuclear Magnetic Resonance (NMR)

^{1}H-NMR spectra of polyesters were obtained with a Bruker spectrometer operating at a frequency of 400 MHz. A sample concentration equal to 5% w/v in deuterated trifluoroacetic acid (d-TFA) was used. The number of scans was 10 and the sweep width was 6 kHz.

2.6. Thermal analysis

TGA measurements were carried out under nitrogen atmosphere using a Perkin Elmer TGA7 apparatus at 10 °C /min heating rate up to 900 °C.

Calorimetric measurements were performed by means of a Perkin Elmer DSC7 instrument. The external block temperature control was set at -60ºC and weighed samples of c.a. 10 mg were encapsulated in aluminum pans and heated up to 40ºC above fusion temperature (T_m) at a rate of 20 ºC/min (first scan), held for 3 min, and then rapidly quenched (about 100 ºC/min) to 0 ºC. Finally, they were reheated from 0 ºC to a temperature well above T_m at the same heating rate (second scan). In order to determine the crystallization rate under non-isothermal conditions, the samples were heated at 20 ºC/min to about 40 ºC above the melting point, kept there for 3 min and then cooled at 5 ºC/min. The measurements were performed under nitrogen atmosphere (10 ml/min). ΔC_p and ΔH_m have been calculated by considering the neat polymer mass.

A TA Instruments temperature modulated DSC (TA Q2000) was also used for the MDSC studies. The instrument was calibrated with indium for the heat flow and temperature, while the heat capacity was evaluated using sapphire standard. Nitrogen gas flow of 50 ml/min was purged into the DSC cell. The sample mass was about 5 mg. The temperature modulated DSC scans (TMDSC) were carried out at a heating rate of 5 ºC/min, with temperature modulation amplitude of 1 ºC and period of 60 s.

2.7. Polarizing Light microscopy (PLM)

A polarizing light microscope (Nikon, Optiphot-2) equipped with a Linkam THMS 600 heating stage, a Linkam TP 91 control unit and a Jenoptic ProgRes C10Plus camera with the Capture Pro 2.1 software were used for PLM observations.

2.8. X-ray diffraction (XRD)

X-ray diffraction (XRD) patterns were carried out by using a PANalyticalX'PertPro diffractometer equipped with a fast solid state X'Celerator detector and a copper target (λ = 0.15418 nm). Data were acquired in the 3.2-60.0° 2θ interval, by collecting 100 sec at each 0.1° step. *In situ* XRD analysis was performed by using an Anton Paar TTK-450 sample stage. The temperature was increased at 20°C/min and the data collection was performed at the temperatures reported on the figures by scanning from 10 to 35° 2θ degrees counting 40s each 0.1° step (with the fast X'Celerator detector an XRD scan was collected in 40s). The 1st temperature scan was performed from 25°C up to 250°C. After 3 min at this temperature, the samples were quenched in liquid nitrogen. The indices of crystallinity (χ_c) were evaluated from the X-ray powder diffraction profiles

by the ratio between the crystalline diffraction area (Ac) and the total area of the diffraction profile (At), $\chi_c = A$c/At. The incoherent scattering was taken in due consideration. The length of crystal domains were estimated by the Scherrer formula (K=1).

3. Results and discussion

3.1. Synthesis and molecular characterization

PEF nanocomposites were *in situ* prepared by melt polycondensation of dimethyl 2,5-furan-dicarboxylate and ethylene glycol in the presence of the nanofillers. Functionalized MWCNTs, original MWCNTs and GO were used as nanofillers. The filler weight content in nanocomposites was in all cases 2.5 wt%. After melt polycondensation, solid state polycondensation (SSP) was performed heating the samples at 200 ºC for 4h under vacuum, in order to increase their molecular weight. The intrinsic viscosity of all samples was measured and is shown in Table 1. It can be seen that almost all materials present similar values of intrinsic viscosities, with the exception of the PEF/MWCNTs-NH$_2$, which has the lowest value. This fact can be explained as due to the nature of the MWCNTs-NH$_2$ as additive. Amino-groups could react with furanic acid and aminolysis reactions could take place and consequently the polymerization degree and the molecular weight may be reduced [59].

Table 1: Intrinsic viscosity of the PEF-based nanocomposites

Polymer	$[\eta]$ (dL/g)
PEF	0.45
PEF/MWCNTs	0.44
PEF/MWCNTs-COOH	0.43
PEF/MWCNTs-NH$_2$	0.39
PEF/GO	0.42

The structure of the prepared nanocomposites was verified with ^{1}H-NMR spectroscopy. The corresponding spectra of neat PEF, PEF/MWCNTs, PEF/MWCNTs-COOH, PEF/MWCNTs-NH$_2$ and PEF/GO are shown in Figure 1. Since the fillers could not be dissolved in the deuterated solvents, the NMR spectra appear to be identical, owing to the detection of the solely PEF structure [27]. In more detail, the "a" protons of the composed polyesters attributed to the furan ring appear at the highest ppm values, 7.42 ppm (2H, s), while the 4 protons of the glycol subunit ("b" protons) appear at 4.80

ppm (4H, s). This result is in accordance with our previous studies [27]. The peak integration was consistent with the chemical structure for each polymer spectrum.
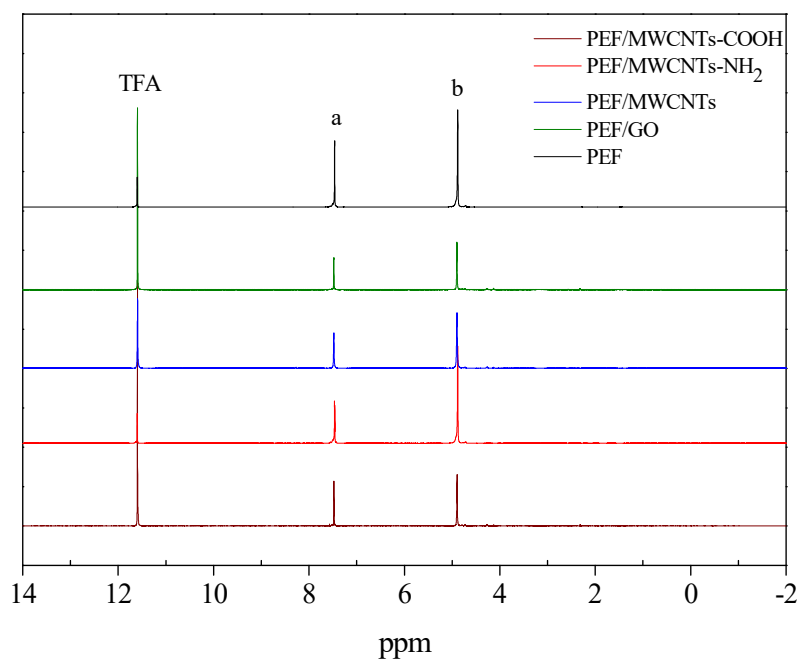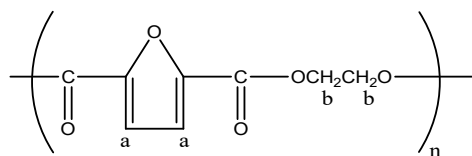

Figure 1: ^{1}H-NMR spectra of the PEF nanocomposites.

These samples were used for further analysis. Furthermore, a part of each sample was solvent treated and purified, as previous studies proved that solvent treated PEF sample crystallized in β-crystal form, whereas melt or cold-crystallized PEF developed a different crystal phase, named α-crystal form [33]. For this reason 10 g of milled PEF were transferred into a beaker where 200 mL of dichloromethane was added. The mixture was stirred until a part of the amount of PEF was dissolved. After filtration, a white-colored material was isolated on the Gooch filter. Neat PEF was kept overnight under vacuum to remove the residue of the used solvent. Both purified and as prepared samples were tested to compare their behaviours.

3.2. Thermal characterization

The thermal stability of the nanocomposites in comparison to the neat PEF was studied by TGA (Figure 2). The temperature values of thermal decomposition onset (T_{id}) as

well as those of the maximum decomposition rate (T_{max}) are summarized in Table 2. It can be seen that all polyesters are thermally stable materials since their decomposition starts after 350 ºC, which is in agreement with our previous studies [60]. However, thermal stability of nanocomposites is decreased with respect to the neat PEF, due to the presence of nanofillers. In particular, the nanocomposites containing MWCNTs-COOH and GO showed the lowest stability. These nanofillers have –COOH and –OH groups, which may interact with PEF macromolecular chains, reducing thermal stability of polyesters. Thus, T_{id} and T_{max} in all samples are lower than neat PEF. Thermal degradation occurred in one step, with the exception of the purified PEF, which shows a first small degradation at around 150 °C, attributable to solvent evaporation. Finally, as it can be seen, a slight decrease of the thermal stability can be highlighted by comparing the purified and not purified nanocomposites, maybe due to the remaining solvent.

Table 2. TGA and 1st DSC scan of PEF-based nanocomposites.

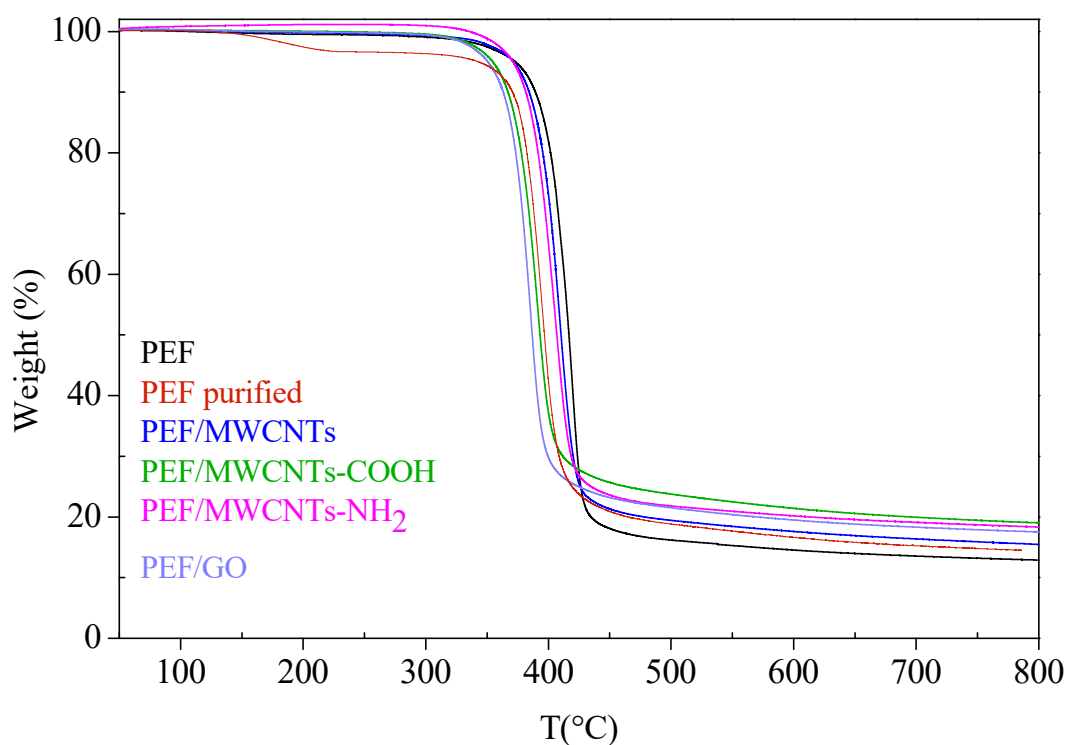| Polymer	T_{id} (°C)	T_{max} (°C)	1stscan, DSC			
			T_{cc} (°C)	ΔH_{cc} (J/g)	T_m (°C)	ΔH_m (J/g)
PEF	401	418	183	3	215	4
PEF/MWCNTs	394	409	--	--	226	46
PEF/MWCNTs-COOH	375	391	--	--	220	38
PEF MWCNTs-NH₂	384	405	--	--	219	39
PEF/GO	370	385	--	--	221	38
Purified Polymer						
PEF	391	404	--	--	219	48
PEF/MWCNTs	393	407	--	--	219	54
PEF/MWCNTs-COOH	373	387	--	--	211	53
PEF/MWCNTs-NH₂	387	406	--	--	209	57
PEF/GO	367	385	--	--	213	49

Figure 2. TGA thermograms of PEF and PEF-based nanocomposites recorded at a heating rate of 10°C/min under N_2 atmosphere.

The thermal transitions of the samples were studied by DSC. As evidenced by the 1st scan, the purified PEF and the nanocomposites are semicrystalline, while the as-synthesized PEF sample is initially amorphous, and is able to crystallize during the heating scan. However, even in this case its ΔH_m is only 4 J/g (Table 2). Among the nanocomposites, original MWCNTs caused the highest increase in the enthalpy of fusion with respect to as-synthesized PEF (Table 2 and Figure 3a). Moreover, in this case the melting peak is particularly sharp, indicating a high perfection of the crystalline phase and a narrow crystal size distribution. On the other hand, functionalized MWCNTs and GO, although acting as nucleating agents for the PEF crystallization, give rise to a lower melting temperature and less crystal perfection than original MWCNTs, as it can be concluded by the lower enthalpy and broader peak of fusion. Figure 3b shows the scans after melt quenching. Both neat PEF and the nanocomposites can be effectively quenched.
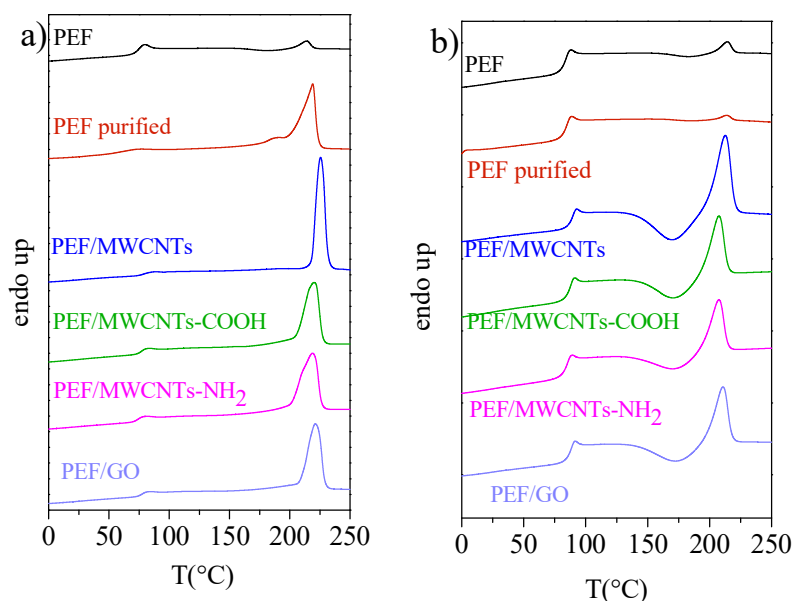
Figure 3. a) 1st scan and b) 2nd scan after melt quenching of PEF and PEF-based nanocomposites.

Table 3 reports the calorimetric data of the DSC scan after melt quenching, together with the temperature corresponding to the maximum of the crystallization peak in cooling experiments (T_c). As it can be seen, all the materials after quenching are amorphous (see Figure 3b). The ability of neat PEF to crystallize during heating is very limited even after solvent treatment, as in the case of untreated sample, while nanocomposites can crystallize to a higher extent. All nanocomposites exhibited a clear cold crystallisation peak, due to the filler ability to act as nucleating agent. This effect is again more evident in the case of not functionalized MWCNTs as the enthalpy of fusion is higher. No differences have been highlighted between the functionalized MWCNTs and GO containing samples.

The behaviour of the purified and not purified samples was also compared. DSC scans of both as prepared and purified PEF/MWCNTs and PEF/MWCNTs-COOH samples are reported in Figure 4 as an example. The solvent treated nanocomposites display a significant increase of crystallinity and a decrease of the melting temperature as compared to the not purified ones. The first effect may be due to solvent-induced crystallization, while the second to the extensive annealing suffered by the as prepared samples during solid state polymerization. Moreover, the melting peak is broader and a shoulder is present in all the purified nanocomposites. Although detailed WAXS analyses will be presented in a following section, it should be noted here that no differences have been highlighted between the WAXS patterns of solvent treated and

12

original nanocomposites. Therefore, the presence of nanofillers led to preferential formation of α-crystals. The DSC heating scans of the solvent treated samples after quenching display a decrease of the cold-crystallization temperature, indicating faster crystallization rates. As to the melting phenomenon after cold crystallization, the T_m did not significantly change with solvent treatment of the nanocomposites, while an increase in the crystallinity can be observed.
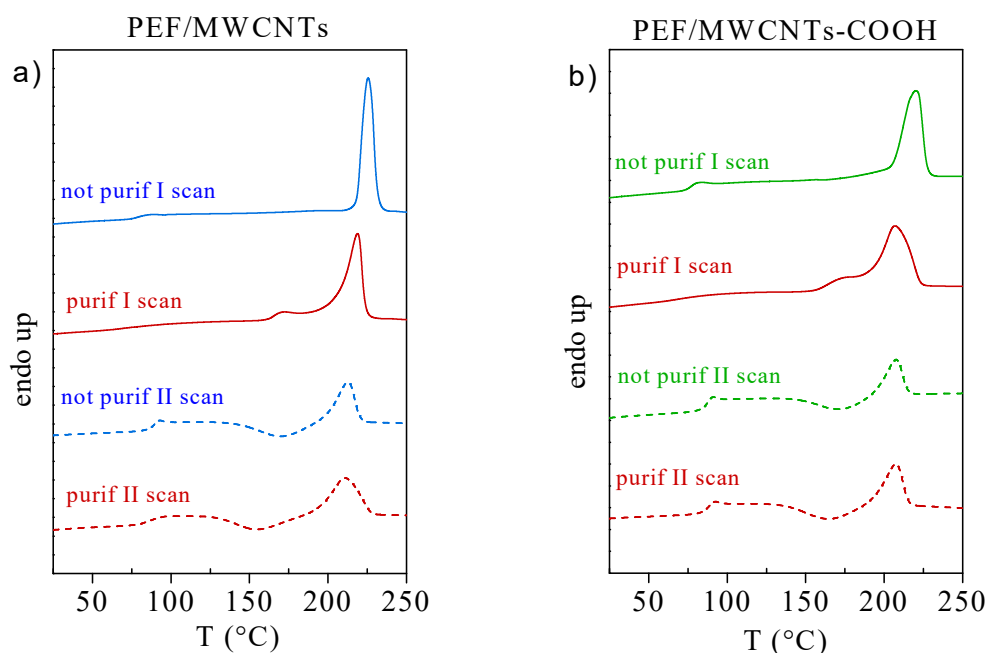

Figure 4. Calorimetric curves of a) PEF/MWCNTs and b) PEF/MWCNTs-COOH. The behaviour of the solvent treated and as prepared samples are compared.

The glass transition values of the purified and not purified samples did not show any significant difference (Table 3). However, in almost all nanocomposites (excluding those with MWCNTs-NH$_2$) the recorded T_g is much higher compared to that of neat PEF.

Table 3. 2nd scan DSC data and controlled cooling from the melt (5°C/min) of PEF and PEF-based nanocomposites.

Polymer	II scan, DSC						
	T_g (°C)	ΔC_p (J/°C·g)	T_{cc} (°C)	ΔH_{cc} (J/g)	T_m (°C)	ΔH_m (J/g)	T_c (°C)
PEF	82	0.416	183	2	214	2	152
PEF/MWCNTs	88	0.300	171	20	213	21	174

PEF/MWCNTs-COOH	86	0.395	172	14	208	14	170
PEF/MWCNTs-NH$_2$	83	0.390	172	12	208	12	167
PEF GO	87	0.381	174	14	211	14	169
Purified polymer							
PEF	83	0.395	185	1	214	1	157
PEF/MWCNTs	87	0.317	155	21	214	30	181
PEF/MWCNTs-COOH	87	0.381	163	14	208	21	178
PEF/MWCNTs-NH$_2$	81	0.405	164	13	207	30	170
PEF/GO	87	0.382	168	16	211	20	172

The nucleating effect given by the nanofillers is confirmed also by the data obtained from cooling scans at a controlled rate (5 °C/min) (Table 3 and Figure 5a). Indeed, the T_c is recorded at higher temperatures for the nanocomposites with respect to the neat PEF. The highest highest T_c among the studied samples corresponds to the PEF/MWCNTs. On the other hand, the lowest T_c is displayed by the sample containing the MWCNTs-NH$_2$, which is also the nanocomposite displaying the lowest enthalpy of fusion and melting temperature after quenching. A similar behaviour was also found in all solvent treated samples. As can be seen from Figure 5b all purified samples were able to crystallize at higher temperatures, compared to un-purified samples.
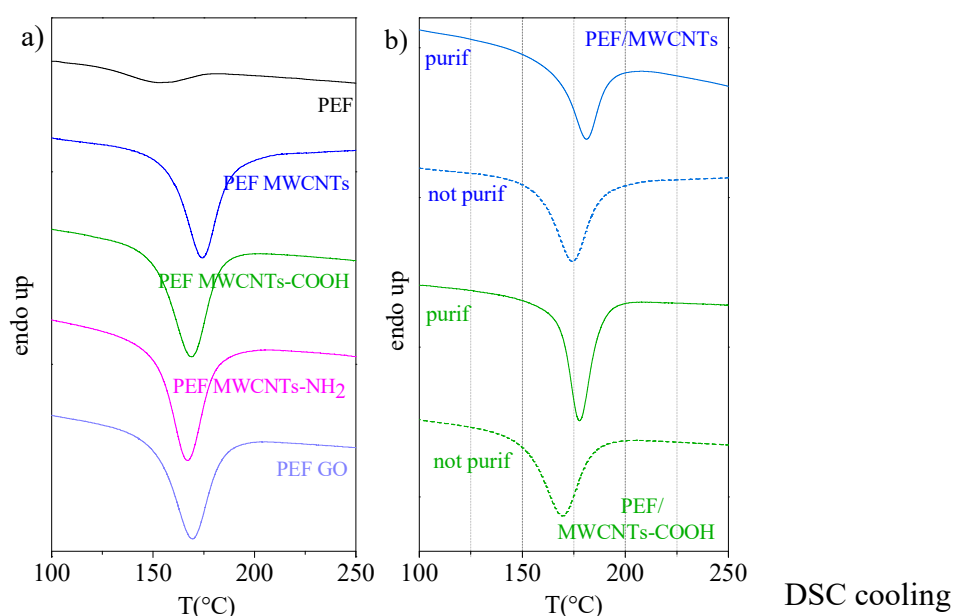

Figure 5. DSC cooling scans at 5°C/min from the melt for a) not purified PEF and nanocomposites, b) original and solvent treated PEF/MWCNTs and PEF/MWCNT-COOH samples.

PLM experiments display an increase of the spherulites number and a drastic decrease in their size for the nanocomposites (supplementary material S1) as compared to neat PEF at 200 ºC. PEF and furanoates in general show rather large nucleation density, as reported in previous works [27]. The temperature of 200 ºC is relatively high, so that the nucleation density for PEF is moderated. Therefore, this is a direct proof of the nucleation efficiency of the fillers. Similar photographs were also taken for the not purified samples (data not presented).

In conclusion, from DSC and PLM studies it was proved that nanofillers act as nucleating agents for the PEF crystallization, although to a different extent. A similar behaviour was observed also in PEF nanocomposites with organo-modified montmorillonite (OMMT) clays [61]. The highest effect was displayed by the sample containing neat MWCNTs, while the lowest one was shown by the sample containing MWCNTs- NH_2. This is because neat MWCNTs are not expected to react with the monomers, but they offer extensive solid surfaces to nucleate polymer crystallization. Furthermore, the addition of nanofillers led to formation of α-crystals.

3.3. Structural characterization

WAXS analyses have been carried out to investigate the crystal structure of the samples. The as-received neat PEF sample is amorphous, while all the nanocomposites show the typical patterns of PEF α-crystalline phase previously reported [33, 28, 32], suggesting an active role of the nanoparticles in the nucleation process of crystal seeds (Figure 6a). The main reflections are at 16.0°, 17.8°, 19.3°, 20.5°, 23.4° and 26.6° (2 theta) and appear very sharp and well resolved from the amorphous bump. From the peak width of the reflections at 16.0° and 17.8° a value of 18±1 nm for the length of crystal domains can be estimated and from the reflections/amorphous area ratio an index of crystallinity of about $37 \pm 2\%$ can be calculated. This is a mean value since the χ_c variations between the samples containing different nanoparticles are within the standard deviation interval.
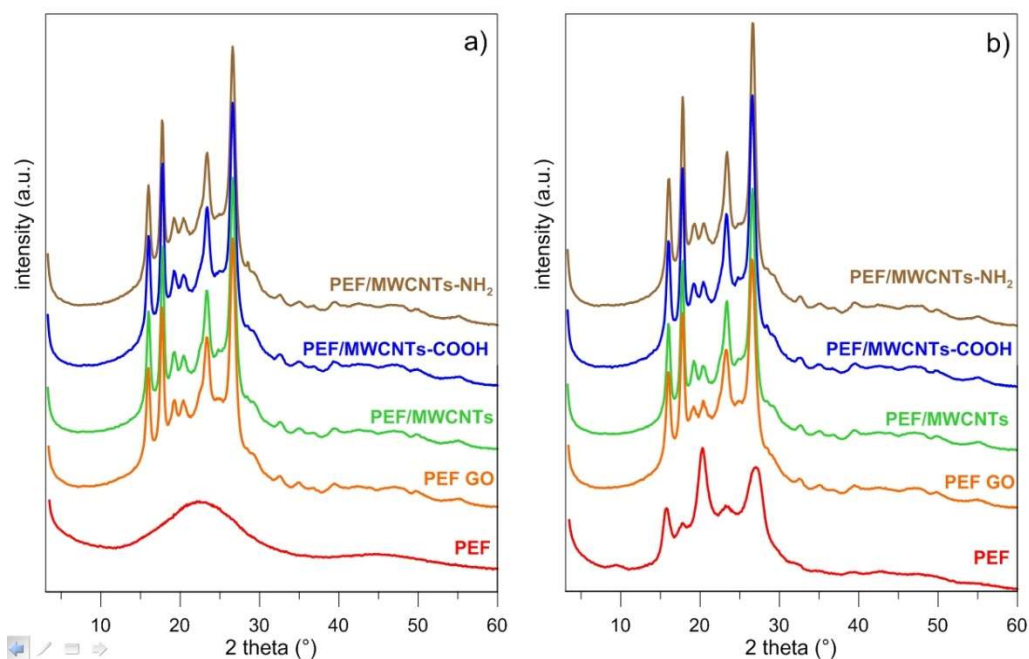
Figure 6. XRD patterns of the PEF nanocomposites. a) as prepared; b) after purification process.

The stability of the crystal phase has been investigated by real time XRD. In Figure 7a are reported the profiles collected during the 1st heating scan of the PEF-MWCNTs nanocomposite taken as an example. The α-phase pattern is maintained during the heating process, but a strong anisotropy of the cell expansion is detected. Indeed, while the peaks at 2-theta 16.0° and 17.8° are still centered at the same position during the heating, the peaks at 23.4° and 26.7° shift to lower angles up to 22.6° and 25.8° (longer distances). The pattern of the molten phase shows an additional 'bump' at 25.1°, which can be ascribed to the filler presence (in Figure S2 is reported the pattern of pure MWCNTs). After melt quenching, a 2nd heating process was followed by XRD. The scans are reported in Figure 7b. At the heating rate used, a crystal phase develops over 130°C, but with the typical pattern of (less stable) PEF α-phase (main reflections at 15.6°, 17.5°, 20.2°, 22.2°, 25.5°). The further melting and slow cooling at controlled rate promotes the formation of the α crystal phase.
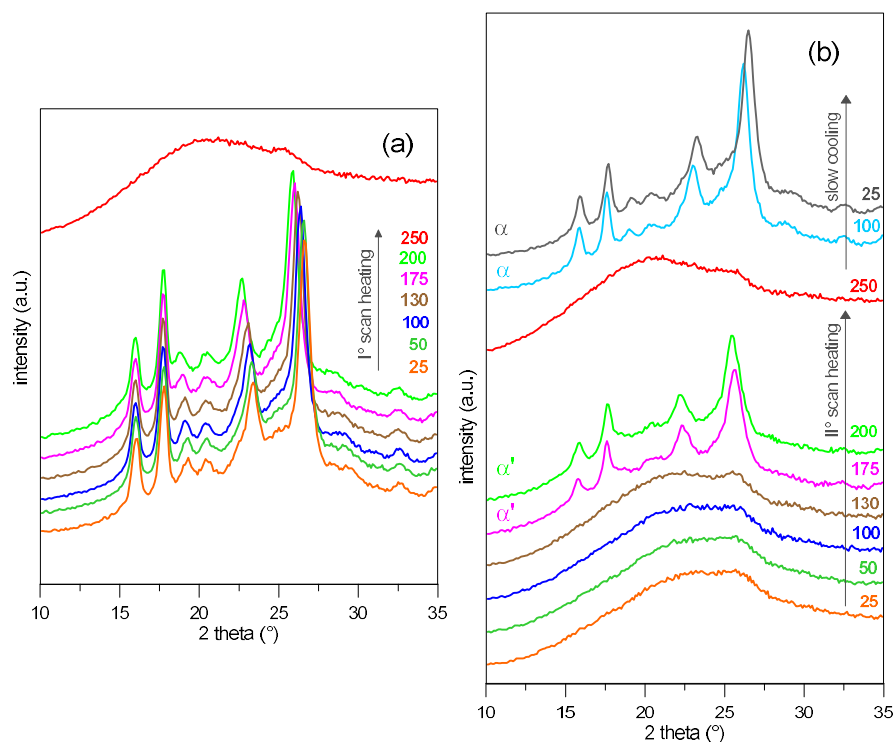
Figure 7. *In situ* variable temperature XRD data (a) Ist heating scan, (b) IInd scan after melt quenching and subsequent slow cooling for the PEF/MWCNTs nanocomposite. The temperature of the data collection is expressed as °C.

The XRD patterns of the purified PEF are consistent with that of β-crystal modification, as expected (Figure 6b). However, all solvent treated nanocomposites show the same patterns of PEF α-phase, as the not treated samples. This means that contrarily to neat PEF sample, the presence of the nanoparticles favours the formation of the α-phase even in case of solvent treatment. The values of crystal domain length and crystallinity are consistent with those found for not treated samples. The study of the phase stability of the purified samples is reported in the Figure S3. The thermal treatment shows the same transformations, suggesting that the solvent treatment does not alter the stability of the nanocomposites.

3.4. Melting behavior study

The melting behavior of the nanocomposites was investigated with MDSC. Figure 8a shows the MDSC signals for neat PEF after melt quenching. The cold crystallization peak temperature appears at 168 °C in the total and non-reversing signal curves. A relatively small recrystallization exotherm follows, while the large melting endotherm dominates in the reversing signal. For the quenched PEF/MWCNT nanocomposite, the

cold-crystallization peak appears at 144.3 °C, and very large recrystallization exotherm starts at 167 °C. These findings confirm that the crystallization and recrystallization of this nanocomposite is promoted by the presence of the nanoparticles. As visible for the nanocomposite containing GO in Figure 9a, a similar behavior with large recrystallization peaks has been observed for the other nanocomposites, although the crystallization rates are not as fast as those of PEF/MWCNTs.
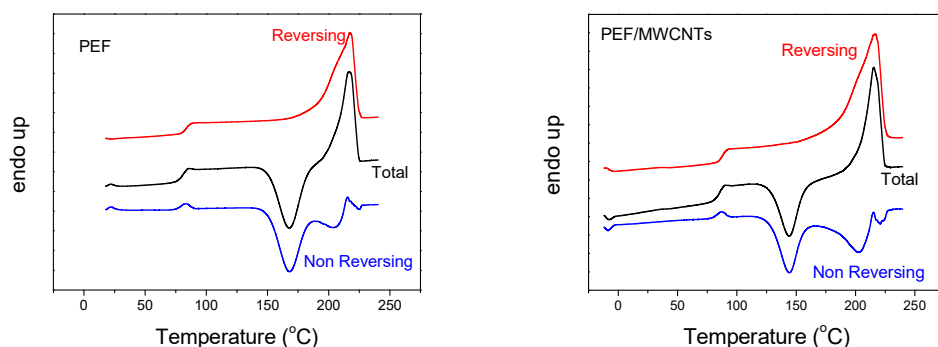

Figure 8. MDSC thermograms for a) quenched PEF and b) quenched PEF/MWCNTs nanocomposites.

The melting of neat PEF and of nanocomposites were studied after crystallization at three different T_cs, namely 140, 165 and 200 °C. PEF GO nanocomposite displayed large recrystallization during MDSC heating after isothermal crystallization at the T_c in the low crystallization temperature region (140 °C for 2 h). This behavior is indicative of the low stability of the original crystals formed at this low T_c. The sample after crystallization at 165 °C for 1 h also showed low crystal stability and large re-crystallization exothermic peak in the non-reversing signal (Figure 9c). This behavior was observed for all the samples including neat PEF. The particular, T_c was chosen as this is the temperature at which PEF shows its maximum crystallization rate [33].

In contrast to previous observations, the sample crystallized at 200 °C (Figure 9d) showed a non-reversing melting. As a matter of fact, at such high T_cs, close to the melting temperature, large perfect crystals can form. Therefore, the recrystallization rates are limited, while melting is much faster. Thus, the final result is an extended non-reversing melting [62, 63].
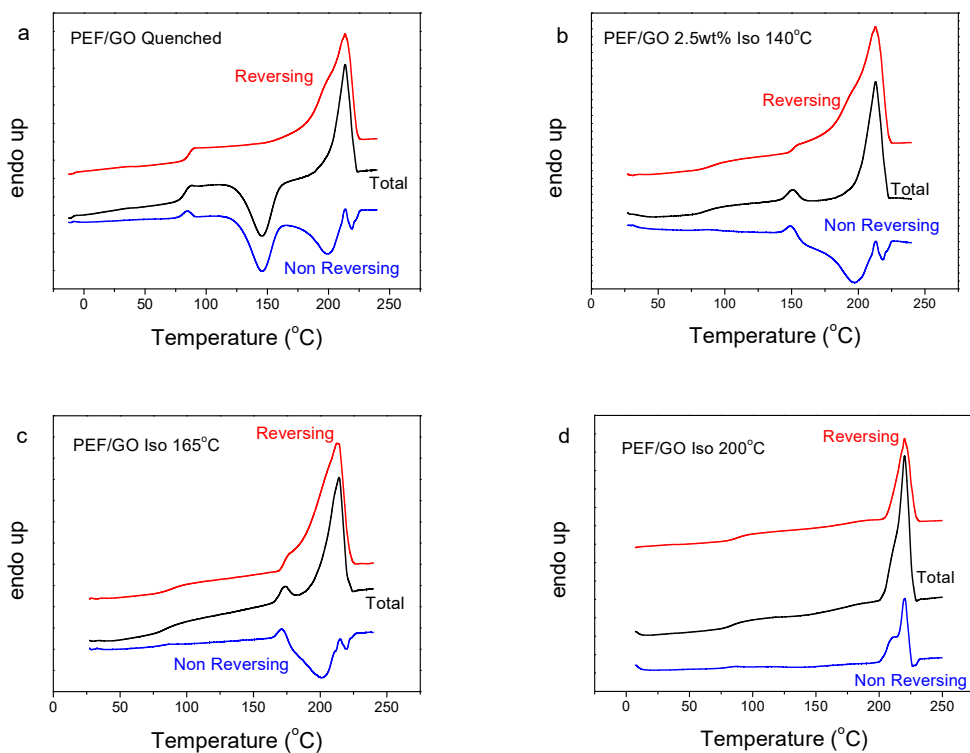
Figure 9. MDSC thermograms for the PEF/GO nanocomposite a) quenched, b), c) and d) crystallized at 140, 165 and 200 °C, respectively.

4. Conclusions

PEF nanocomposites containing 2.5 wt% MWCNTs, functionalized MWCNTs with -COOH or -NH$_2$, or GO were in situ prepared by melt polycondensation. Solid state polycondensation was also applied to increase the molecular weight of the samples. Molecular characterization of the samples indicated that a good control and optimization of the nanocomposite preparation method was achieved. Thermal properties evaluation indicated that all the fillers acted as nucleating agents for the PEF crystallization, but to a different extent. Indeed, the nanocomposites containing MWCNTs showed the highest melting temperature and the highest enthalpy of fusion among the tested nanocomposites. On the other hand, the composite with MWCNT-NH$_2$ showed the lowest thermal performance including crystallization and thermal stability. The addition of nanoparticles, whatever their nature, promoted the formation of PEF α-crystal phase. While solvent treated PEF displayed the formation of β-crystal phase, in the nanocomposites thermal and solvent treatments were not capable of

inducing the same transformation, as only α-crystal reflections were displayed. This is a clear indication that the addition of different nanofillers to PEF matrix always favors the formation of the α-crystal phase. Although further studies are necessary to fully evaluate the potentialities of PEF nanocomposites, we believe that the present results can serve as a starting point and a guide for further investigations, due to the high interest in the PEF from both the scientific and industrial community as a more sustainable alternative to PET.

References

1. T. Werpy, G. Petersen, Top Value Added Chemicals from Biomass: Volume I- Results of Screening for Potential Candidates from Sugars and Synthesis Gas. Aug 2004 (http://www.nrel.gov/docs/fy04osti/35523.pdf).

2. T. Pan, J. Deng, Q. Xu, Y. Zuo, Q.-X. Guo, Y. Fu, ChemSusChem 6 (1) (47-50) 2013.

3. S. Yoshida, K. Hiraga, T. Takehana, I. Taniguchi, H. Yamaji, Y. Maeda, K. Toyohara, K. Miyamoto, Y. Kimura, K. Science, 351 (1196-1199) 2016.

4. J. G. N. Drewitt, J. Lincoln, G.B. Patent 621, 1946, pp. 971.

5. A. Gandini. Adv. Polym. Sci. 25 (49–96) 1977.

6. J. A. Moore, J. E. Kelly, Macromolecules 11 (568-573) 1978.

7. E. de Jong, M. A. Dam, L. Sipos, G.-J. M. Polym. Mater., 1105 (1–13) 2012.

8. A. Gandini, A. J. D. Silvestre, C. P. Neto, A. F. Sousa, M. Gomes. J. Polym. Sci.: Polym. Chem. 47 (295–298 2009.

9. R.J.I. Knoop, W. Vogelzang, J. van Haveren, D.S. van Es J. Polym. Sci. Part A: Polym. Chem.,51 (4191-4199) 2013.

10. M. Soccio, M. Costa, N. Lotti, M. Gazzano, V. Siracusa, E. Salatelli, P. Manaresi, A. Munari. Eur. Polym. J. 81 9397–412, 2016.

11. M. Gomes, A. Gandini, A.J.D. Silvestre, B. Reis. J. Polym. Sci.: Polym. Chem. 49 (3759–3768) 2011.

11. J. Ma, X. Yu, J. Xu, Y. Pang. Polymer, 53 (4145-4151) 2012.

12. M. Jiang, Q. Liu, Q. Zhang, C. Ye, G. Zhou. J. Polym. Sci. Polym. Chem. 50 (1026–1036) 2012

13. J. Ma, Y. Pang, M. Wang, J. Xu, H. Ma, X. Nie. J. Mater. Chem. 22 (3457–3461) 2012.

14. L. Wu, R. Mincheva, Y. Xu, J.M. Raquez, P. Dubois. Biomacromolecules 14 (890-899) 2013.

15. P. Gopalakrishnan, S. Narayan-Sarathy, T. Ghosh, K. Mahajan, M.N. Belgacem. J. Polym. Res. 21 (1-9) 2014.

16. S. Thiyagarajan, W. Vogelzang, R.J. Knoop, A.E. Frissen, J. van Haveren, D.S. van Es. Green Chemistry 16 (1957-1966) 2014.

17. M. Matos, A.F. Sousa, A.C. Fonseca, C.S.R. Freire, J.F.J. Coelho, A.J.D. Silvestre. Macromol. Chem. Phys. 215 (2175–2184) 2014.

18. N. Jacquel, R. Saint-Loup, J.P. Pascault, A. Rousseau, F. Fenouillot. Polymer 59 (234–242) 2015.

19. B. Wu, Y. Xu, Z. Bu, L. Wu, B.G. Li. Polymer, 55 (3648–3655) 2014.

20. C.H.R.M. Wilsens, J.M.G.A. Verhoeven, B.A.J. Noordover, M.R. Hansen, D. Auhl, S. Rastogi. Macromolecules, 47 (3306–3316) 2014.

21. C.H.R.M. Wilsens, B.A.J. Noordover, S. Rastogi. Polymer, 55 (2432–2439) 2014.

22. V. Tsanaktsis, G.Z. Papageorgiou, D.N. Bikiaris. J. Polym. Sci. Part A, Polym. Chem., 53 (2617-2632) 2015.

23. V. Tsanaktsis, Z. Terzopoulou, M. Nerantzaki, G.Z. Papageorgiou, D.N. Bikiaris. Mater. Lett. 178 (64-67) 2016.

24. S.K. Burgess, O. Karvan, J.R. Johnson, R.M. Kriegel, W.J. Koros. Polymer 55 (4748-4756) 2014.

25. S.K. Burgess, C.R. Mubarak, R.M. Kriegel, W.J. Koros. J. Polym. Sci. Part B: Polym. Phys. 53 (389-399) 2015.

26. S.K. Burgess, R.M. Kriegel, W.J. Koros. Macromolecules 48 (2184-2193) 2015.

27. G.Z. Papageorgiou, V. Tsanaktsis, D.N. Bikiaris, Phys. Chem. Chem. Phys. 16 (7946-7958) 2014.

28. J.G. van Berkel, N. Guigo, J.J. Kolstad, L. Sipos, B. Wang, M.A. Dam, N. Sbirrazzuoli. Macromol. Mater. Eng. 300 (466-474) 2015.

29. A. Codou, N. Guigo, J. van Berkel, E. De Jong, N. Sbirrazzuoli. Macromol. Chem. Phys. 215 (2065-2074) 2014.

30. A. Codou, M. Moncel, J.G. van Berkel, N. Guigo, N. Sbirrazzuoli, Phys. Chem. Chem. Phys., DOI: 10.1039/C6CP01227B accepted manuscript.

31. L.G. Kazaryan, F.M. Medvedeva. Vysokomolekulyarnye Soedineniya, Seriya B: Kratkie Soobshcheniya, (305-306) 1968.

32. G. Stoclet, G.G. du Sart, B. Yeniad, S. de Vos, J. Lefebvre. Polymer 72 (165-176) 2015.

33. V. Tsanaktsis, D.G. Papageorgiou, S. Exarhopoulos, D.N. Bikiaris, G.Z. Papageorgiou, Cryst. Growth Des. 15 (5505-5512) 2015.

34. A.K. Haernvall, C.M. Pichler, G. Ghazaryan, R. Breinbauer, G.M. Guebitz. J. Biotechn., In Press.

35. A. Sanz, A. Nogales, T.A. Ezquerra, W. Häussler, M. Soccio, N. Lotti, A. Munari. Macromolecules 44 (8124-8128) 2011.

36. M.Gigli, N. Lotti, V. Siracusa, M. Gazzano, A. Munari, M.D. Rosa, Eur. Polym. J. 78 (314–325) 2016.

37. S. Aoyama, Y.T. Park, T. Ougizawa, C.W. Macosko, Polymer, 55 (2077-2085) 2014.

38. A. Sanz, A. Nogales, T.A. Ezquerra, M. Soccio, A. Munari, N. Lotti. Macromolecules, 43 (671-679) 2010.

39. L. Martino, V. Niknam, N. Guigo, J.G. van Berkel, N.Sbirrazzuoli, RSC Adv. 6 959800-59807) 2016.

40. G.D. Barber, B.H. Calhoun, R.B. Moore. Polymer 46 (6706-6714) 2005.

41. C.I.W. Calcagno, C.M. Mariani, S.R. Teixeira, R.S. Mauler, Polymer, 48 (966-974) 2007.

42. Y. Wang, J. Gao, Y. Ma, U.S. Agarwal, Composites: Part B 37 (399–407) 2006.

43. D.W. Litchfield, D.G. Baird. Polymer 49 (5027–5036) 2008.

44. H. Kim, A.A. Abdala, C.W. Macosko, Macromolecules 43 (6515–6530) 2010.

45. S.S. Ray, M. Okamoto, Prog. Polym. Sci. 28 (1539–1641) 2003.

46. M. Moniruzzaman, K.I. Winey. Macromolecules 39 (5194–5205) 2006.

47. Z. Spitalsky, D. Tasis, K. Papagelis, C. Galiotis. Prog. Polym. Sci. 35 (357–401) 2010.

48. T. Ramanathan, A.A. Aabdala, S. Stankovich, D.A. Dikin, M. Herrera-Alonso, R.D. Piner, D.H. Adamson, H.C. Schniepp, X. Chen, R.S. Ruoff, S.T. Nguyen, I.A. Aksay, R.K. Prud'Homme, L.C. Brinson. Nature Nanotechn. 3 (327 – 331) 2008.

49. A.K. Geim, K.S. Novoselov. Nat .Mater. 6 (183–191) 2007.

50. S. Park, R.S. Ruoff. Nat. Nanotech. 4 (217–224) 2009.

51. B.Z. Jang, A. Zhamu. J. Mater. Sci. 43 (5092–50101) 2008.

52. J.M. Allen, V.C. Tung, R.B. Kaner, Chem. Rev. 110 (132–145) 2010.

53. R. Sengupta, M. Bhattacharya, S. Bandyopadhya, A.K. Bhowmick. Prog. Polym. Sci. 36 (638–670) 2011.

54. S. Stankovich, D.A. Dikin, G.H.B. Dommett, K.M. Kohlhaas, E.J. Zimney, E.A. Stach, R.D. Piner, S. Binh, T. Nguyen, R.S. Ruoff. Nature 442 (282-286) 2006.

55. D.R. Dreyer, S. Park, C.W. Bielawski, R.S. Ruoff. Chem. Soc. Rev. 39 (228–240) 2010.

56. S. Park, R.S. Ruoff. Nature Nanotechn. 4 (217-224) 2009.

57. T. Kuila, S.Bose, A.K. Mishra, P. Khanra, N.H. Kim, J.H. Lee. Prog. Mater. Sci. 57 (1061–11050) 2012.

58. D. Bikiaris, A. Vassiliou, K. Chrissafis, K.M. Paraskevopoulos, A. Jannakoudakis, A. Docoslis. Polym. Degrad. Stab. 93 (952-967) 2008.

59. E. Roumeli, D.G. Papageorgiou, V. Tsanaktsis, Z. Terzopoulou, K. Chrisafis, A. Avgeropoulos, D.N. Bikiaris, ACS Appl. Mater. Interf. 7 (11683-11694) 2015.

60. V. Tsanaktsis, E. Vouvoudi, G.Z. Papageorgiou, D.G. Papageorgiou, K. Chrissafis, D.N. Bikiaris, J. Anal. Appl. Pyrol. 112 (369–378) 2015.

61. L. Martino, V. Niknam, N. Guigo, J.G. van Berkel, N. Sbirrazzuoli. RSC Adv. 6 (59800–59807) 2016.

62. G.Z. Papageorgiou, V. Tsanaktsis, D.G. Papageorgiou, S. Exarhopoulos, M. PapageorgioU, D.N. Bikiaris. Polymer 55 (3846-3858) 2014.

63. B.B. Sauer, W.G. Kampert, E.N. Blanchard, S.A. Threefoot, B.S. Hsiao. Polymer 41 (1099−1108) 2000.
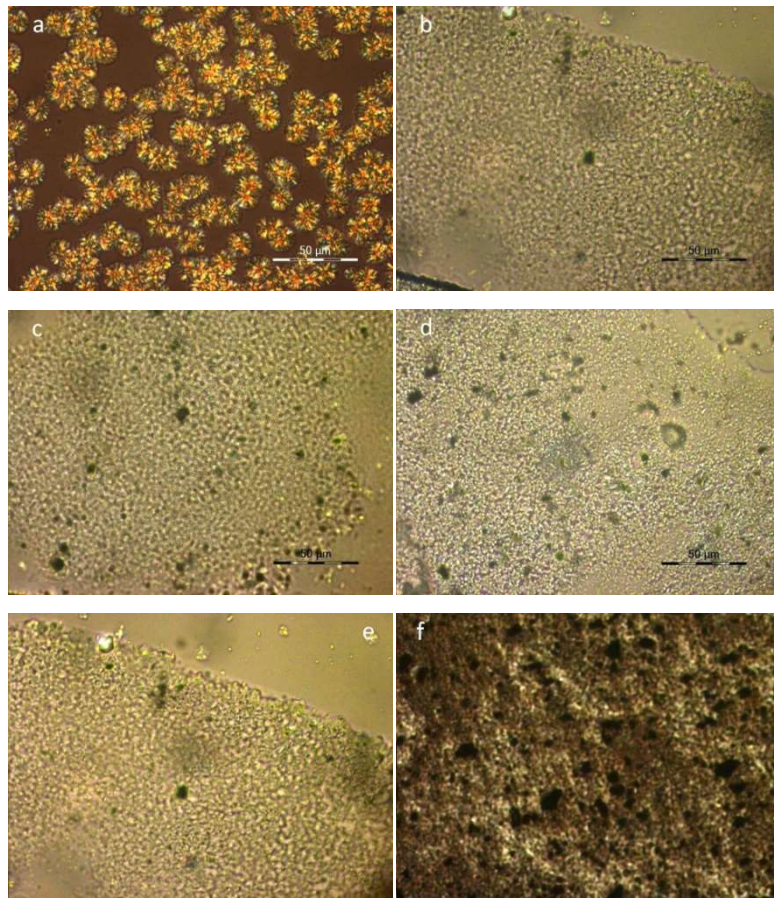
Supplementary material

Figure S1. PLM photographs of neat PEF and nanocomposites after crystallization at 200 ^{o}C a) neat PEF, b) PEF/MWCNTs, c) PEF/MWCNTs-COOH, d) PEF/MWCNTs-NH$_2$, e) PEF/GO and f) PEF/MWCNTs (thick film).
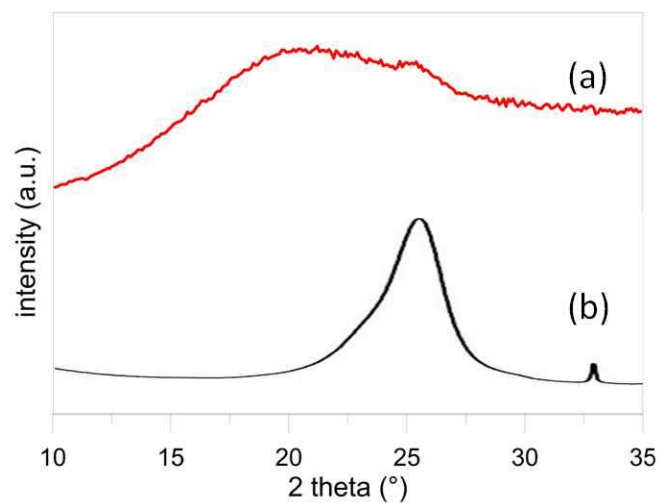
Figure S2. Comparison between the XRD patterns of (a) melt PEF/MNCWTs sample at 250°C and (b) a pure MNCWTs sample.
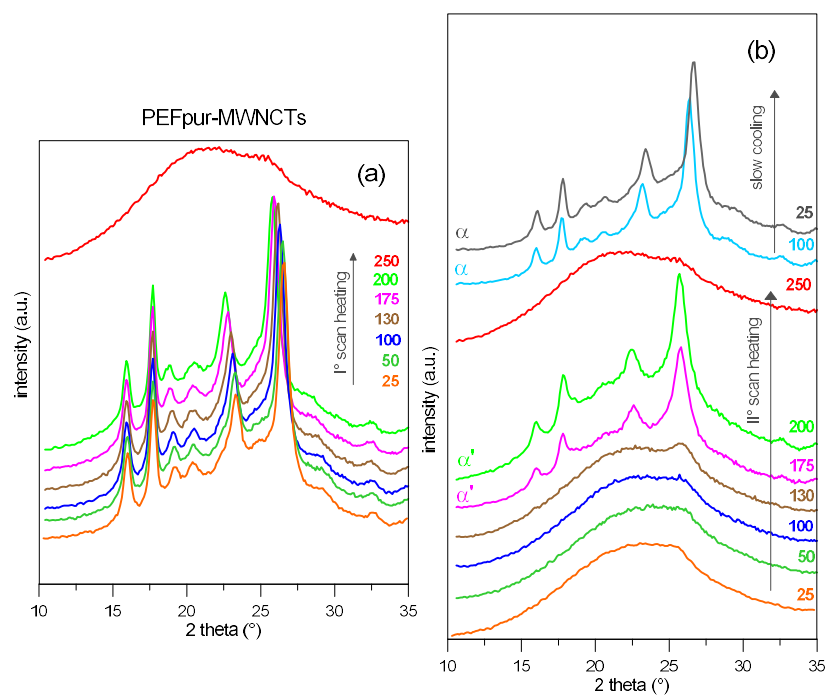

Figure S3. *In situ* variable temperature XRD of the solvent treated PEF/MWCNTs nanocomposite: (a) 1st heating scan, (b) 2nd scan after melt quenching and subsequent slow cooling. The temperature of the data collection is expressed as °C.